

# Quantum entanglement distribution with hybrid parity gate

Feng Mei,<sup>1</sup> Ya-Fei Yu,<sup>1</sup> Xun-Li Feng,<sup>1,2</sup> Zhi-Ming Zhang,<sup>1,2,\*</sup> and C. H. Oh<sup>2</sup>

<sup>1</sup>Laboratory of Photonic Information Technology, SIPSE & LQIT,  
South China Normal University, Guangzhou 510006, China

<sup>2</sup>Centre for Quantum Technologies and Department of Physics,  
National University of Singapore, 3 Science Drive 2, Singapore 117543, Singapore

(Dated: February 25, 2019)

We propose a scheme for entanglement distribution among different single atoms trapped in separated cavities. In our scheme, by reflecting an input coherent optical pulse from a cavity with a single trapped atom, a controlled phase-shift gate between the atom and the coherent optical pulse is achieved. Based on this gate and homodyne detection, we construct an  $n$ -qubit parity gate and show its use for distribution of a large class of entangled states in one shot, including the GHZ state  $|GHZ_n\rangle$ , W state  $|W_n\rangle$ , Dicke state  $|D_{n,k}\rangle$  and certain sums of Dicke states  $|G_{n,k}\rangle$ . We also show such distribution could be performed with high success probability and high fidelity even in the presence of channel loss.

PACS numbers:

## I. INTRODUCTION

In quantum information science, quantum networks play an important role, which can accomplish tasks that are impossible in the realm of classical physics. Quantum networks are composed of quantum nodes for storing and processing information and quantum channels that link the nodes [1]. Distributing entanglement over different nodes through quantum channels is a critical requirement, which could allow physical implementation of quantum cryptography [2, 3], quantum secret sharing [4] and distributed quantum computation (QC) [5]. It has also been found applications in quantum metrology [6] and simulating quantum many-body physics [7]. Many protocols have been proposed for such distribution, including the distribution between two distant single atoms [8, 9], ions [10], atomic ensembles [11] and NV centers [12]. These distributed protocols have high fidelities, but they all rely on postselection by using single-photon detection with very low success probabilities.

An alternative way is to use coherent light instead of single-photon as quantum channels. This way also uses postselection but with homodyne detection of a coherent light. Because the homodyne detection could be done with near-unit efficiency [13], so this distributing way has a high success probability. It has been proposed recently to realize a quantum repeater [14, 15]. In the proposal, through a bright coherent optical pulse sequentially interacting with two electronic spins placed in cavities, entanglement can be distributed between two distant spins by a homodyne detection of the final outgoing coherent pulse, with the fidelity determined by the distinguishability  $d \approx \alpha\theta$  [14, 15]. However, the nonlinear phase shift  $\theta$  of the coherent light pulse generated by the dispersive light-matter interaction in [14, 15] is very small

( $\sim 10^{-2}$ ). Considering the saturation effect, the fidelity can be improved to modest level at most by increasing the amplitude of the coherent light  $\alpha$ . Moreover, this proposal only can project the two distant spins into a Bell state with a probability of success 1/2. In this paper, with single atoms trapped in separated cavities as quantum nodes and a coherent light as quantum channel, we propose a scheme for entanglement distribution among two different nodes by a two-qubit parity gate. Because the parity gate in our scheme relies on both the discrete atomic qubit state and the continuous quantum variable of coherent light amplitude, we call it hybrid parity (HP) gate. The basic building block of the HP gate is a local controlled phase-shift (CPS) gate between a single atom trapped in a cavity and an input coherent light. Based on two local CPS gates and a homodyne detection of the final output coherent optical pulse, one can achieve a two-qubit HP gate. Compared with the proposal [14, 15], the nonlinear phase shift  $\theta$  of the coherent light in the CPS gate is huge and can approach the order of  $\pi$ , which means that the entanglement distribution in our scheme is with high fidelity. Besides, the two distant atoms can be projected into a Bell state in one shot using the HP gate. It is also found that the phase shift could be tuned to realized a  $n$ -qubit HP gate.

With such  $n$ -qubit HP gate, we can distribute a large class of multiqubit entanglement in one shot, like  $n$ -qubit GHZ state  $|GHZ_n\rangle$ , W state  $|W_n\rangle$ , Dicke state  $|D_{n,k}\rangle$ , and certain sums of Dicke states  $|G_{n,k}\rangle$ . These states are essential in some quantum information processing (QIP) protocols, which cover quantum dense coding [16], quantum key distribution [17], quantum teleportation [18], quantum telecloning [19], quantum secret sharing ( $|G_{n,k}\rangle$ ) [20] and scalable quantum search ( $|D_{n,n/2}\rangle$ ) [21]. We also show that our scheme inherits both the advantages of the single photon and coherent light quantum channel based entanglement distribution protocols and could be performed with a high fidelity and high success probability. In addition, compared with the ear-

---

\*Electronic address: zmzhang@scnu.edu.cn

lier QC protocols using cavity input-output process [22–25], our scheme does not require high- $Q$  cavity working in the strong coupling regime and not employ single-photon source, which greatly relaxes the experimental requirement.

This paper is organized as follows. In Sec. II we concretely describe the basic building block in our scheme. Through reflecting an input coherent optical pulse from a cavity with a single trapped atom, we achieve a CPS gate between the atom and the coherent optical pulse. Based on series of CPS gates, an  $n$ -qubit HP gate is constructed in Sec. III. In Sec. IV, we show how to realize the HP gate and use it for entanglement distribution in detail. Finally, we end the paper with a discussion and conclusion in Sec. V.

## II. BASIC BUILDING BLOCK

The basic building block for our scheme is shown in Fig. 1(a), in which a three-level atom is trapped in a single-side cavity. The qubit is represented by different hyperfine levels  $|0\rangle$  and  $|1\rangle$  in the atomic ground-state manifold (see Fig. 1(b)). The atomic transition  $|1\rangle \leftrightarrow |e\rangle$  is coupled to the cavity mode  $a$  and driven by the input field. While the state  $|0\rangle$  is decoupled to the cavity mode due to the large hyperfine splitting. In the rotating frame with respect to the frequency of input pulse, the interaction between the atom and the cavity mode is described by the Hamiltonian

$$H = \delta_1 |e\rangle \langle e| + \delta_2 a^\dagger a + g(a\sigma_+ + a^\dagger\sigma_-), \quad (1)$$

where  $\sigma_+ = |e\rangle \langle 1|$ ,  $\sigma_- = |1\rangle \langle e|$ ,  $\delta_1 = \omega_0 - \omega_p$ ,  $\delta_2 = \omega_c - \omega_p$ ;  $\omega_0$ ,  $\omega_c$  and  $\omega_p$  denote the resonant frequency between the excited state  $|e\rangle$  and the ground state  $|1\rangle$ , the frequency of cavity mode and the input pulse, respectively;  $g$  is the atom-cavity coupling rate. The cavity mode  $a$  is driven by the input field  $a_{in}$ . By omitting the Langevin noises that have negligible contribution to the dynamics, we can easily obtain the Heisenberg-Langevin equations for the internal cavity field and the atomic operator

$$\begin{aligned} \dot{a} &= -\left(i\delta_2 + \frac{\kappa}{2}\right)a - ig\sigma_- - \sqrt{\kappa}a_{in} \\ \dot{\sigma}_- &= -\left(i\delta_1 + \frac{\gamma}{2}\right)\sigma_- + ig\sigma_z a \end{aligned} \quad (2)$$

where  $\kappa$  and  $\gamma$  are the cavity decay rate and the spontaneous emission rate for the excited level,  $\sigma_z = |e\rangle \langle e| - |1\rangle \langle 1|$ . The output field  $a_{out}$  is connected with the input by the standard cavity input-output relation  $a_{out} = a_{in} + \sqrt{\kappa}a$ . The input field has the standard commutation relations  $[a_{in}(t), a_{in}^\dagger(t')] = \delta(t - t')$ . Providing the cavity decay rate  $\kappa$  is sufficiently large, the atom will have a weak excitation. So the component  $|e\rangle \langle e|$  is negligible. Under this approximation,  $-\sigma_z$  can be replaced with the

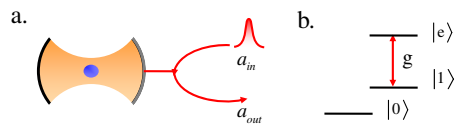


FIG. 1: (Color online) (a) Setup for the basic building block. An input weak coherent optical pulse is reflected by a cavity with a single trapped atom. (b) Level structure of the single-atom and the coupling induced by cavity field.

population  $P_1$  for the atom in the state  $|1\rangle$ . If  $\delta_1 \gg \gamma/2$ , from Eq. (2), we can derive the output field

$$a_{out} = r a_{in}, \quad (3)$$

where the reflection coefficient is

$$r = \frac{i\delta_1(i\delta_2 - \frac{\kappa}{2}) + P_1 g^2}{i\delta_1(i\delta_2 + \frac{\kappa}{2}) + P_1 g^2}. \quad (4)$$

Note that the population  $P_1 = 0$  ( $P_1 = 1$ ) for the atom in the state  $|0\rangle$  ( $|1\rangle$ ). We further define  $r_0$  and  $r_1$  as the reflection coefficient corresponding to the atomic states  $|0\rangle$  and  $|1\rangle$ , and assume that the initial input optical pulse is prepared in a coherent state  $|\alpha\rangle$ , and the atom is initialized in a superposition state. The coherent state can be written in the form of displacement operator, then the initial state of the system is

$$\begin{aligned} |\chi\rangle_i &= \frac{|0\rangle + |1\rangle}{\sqrt{2}} D(\alpha) |0\rangle_{in} \\ &= \frac{|0\rangle + |1\rangle}{\sqrt{2}} e^{\alpha a_{in}^\dagger - \alpha^* a_{in}} |0\rangle_{in}. \end{aligned} \quad (5)$$

After interacting with the cavity-atom system, the input optical pulse will be transformed according to the reflection coefficient. That is, if the atom is in the state  $|0\rangle$ , the relationship between the output field and the input field is  $a_{out} = r_0 a_{in}$  ( $r_0$  is a complex number), then we can get a cavity-assisted transformation for the input coherent field with  $a_{in}^\dagger \rightarrow r_0 a_{out}^\dagger$ . While in the state  $|1\rangle$ , the cavity-assisted transformation for the input coherent field is  $a_{in}^\dagger \rightarrow r_1 a_{out}^\dagger$ . By applying this cavity-assisted transformations on the initial state  $|\chi\rangle_i$ , one can get the final state

$$\begin{aligned} |\chi\rangle_f &= \frac{1}{\sqrt{2}} (|0\rangle D(r_0\alpha) + |1\rangle D(r_1\alpha)) |0\rangle_{out} \\ &= \frac{1}{\sqrt{2}} (|0\rangle |\alpha e^{i\varphi_0}\rangle_{out} + |1\rangle |\alpha e^{i\varphi_1}\rangle_{out}), \end{aligned} \quad (6)$$

where  $\varphi_s = \arg(r_s)$ ,  $s = 0, 1$ . As we can see, with the input-output process, a phase shift conditioned on the atomic state is generated on the input coherent optical

pulse, which yields a controlled phase-shift (CPS) gate. This also extends the QC protocols [26–28] with low- $Q$  cavity and single-photon pulse to continuous variable regime. In the following section, based on series of CPS gates, we will construct an  $n$ -qubit HP gate and use it for distributed quantum computation.

### III. HYBRID PARITY GATE

In order to have a better understanding of the HP gate in our scheme, a brief overview of the parity gate is given firstly. The parity gate has been firstly proposed in linear-optic system to construct a controlled-NOT (CNOT) gate probabilistically [29]. Soon afterwards Beenakker and coauthors have shown that two charge parity gates with single qubit gates can realize a CNOT gate deterministically [30], which is a significant breakthrough for universal QC. These achievements have stimulated great interest to implement a parity gate in various systems for quantum information processing [31]. Now we give a brief introduction for the parity gate. It can be viewed in the following implementation manner

$$|xy\rangle|0\rangle \rightarrow |xy\rangle|x \oplus y\rangle, \quad (7)$$

where  $x$  and  $y$  are the two input qubits, and an ancilla is introduced and initialized firstly in the null state. The gate keeps the input state  $|xy\rangle$  unchanged, but reveals the parity  $\mathbf{p} = x \oplus y$  ( $\oplus$  is the addition mod 2) by measuring the ancilla. If the input state is in the product state  $|+\rangle^{\otimes 2}$ , where  $|+\rangle = (|0\rangle + |1\rangle)/\sqrt{2}$ , the measurement result  $\mathbf{p} = 0$  projects the input state into an entangled state  $(|00\rangle + |11\rangle)/\sqrt{2}$ , and  $\mathbf{p} = 1$  into  $(|01\rangle + |10\rangle)/\sqrt{2}$ . A standard quantum network for the parity gate has been studied in [32], which uses a qubit as an ancilla. Each input qubit interacts once with the ancillary qubit via a CNOT gate. Finally the parity gate is achieved by measuring the ancillary qubit state. This network could be carried out in a photonic module [33].

Recently, Ionicioiu *et al.* have generalized the above parity gate to  $n$ -qubit case [34]. In their generalized parity (GP) module, a qudit with  $d$  dimensional Hilbert space serves as an ancilla. Each qubit interacts once with the ancillary qudit by a controlled- $U$  gate, and  $U (\in U(d))$  is a unitary transformation. For different initial states of the qubits (i.e. with different parities), after series of controlled- $U$  gates, the final qudit states are orthonormal with each other. If the input state is  $\otimes_{i=1}^n |x_i\rangle$  ( $x_i = 0, 1$ ), the generalized parity could be defined as  $\mathbf{p} = \sum_{i=1}^n x_i \bmod d$ , which relies on the measurement outcome of the final qudit state. The authors considered both the nondegenerate ( $n = d$ ) and degenerate case ( $n > d$ ) and showed how to generate entanglement in the two cases. The key demand of this GP module is a controlled- $U$  gate between a qubit and a qudit. The gate is also required to make the final qudit states orthonormal with each other for different parities states of

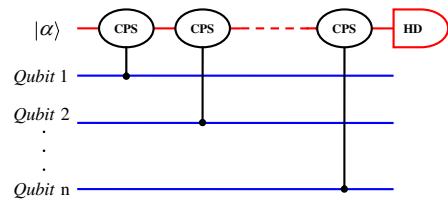


FIG. 2: (Color online) An  $n$ -qubit hybrid parity gate. HD is a homodyne detection on the final output phase-shift coherent state.

qubits. However, it is very difficult to look for such qudit candidate in practice.

Here we further relax this constraint and employ the continuous quantum variable instead of discrete variable as an ancilla. In our scheme, a coherent optical pulse is used as an ancilla, and  $n$  single atoms are the input qubits. Each single atom is trapped in a cavity and interacts once with the input coherent optical pulse by a CPS gate. As shown in Fig. 2, the parity gate acts as

$$\otimes_{i=1}^n |x_i\rangle |\alpha\rangle \rightarrow \otimes_{i=1}^n |x_i\rangle |\alpha(\mathbf{p})\rangle, \quad (8)$$

where  $x_i$  is the  $i$ th input qubit,  $|\alpha\rangle$  is the initial input ancillary coherent state, and  $|\alpha(\mathbf{p})\rangle$  is the final output phase shift coherent state. The parity here is defined as  $\mathbf{p} = \sum_{i=1}^n x_i \bmod n$ , which corresponds to the nondegenerate case in the GP module [34]. As we will demonstrate in detail in the next section, the phase shift of the final output coherent state could reveal the parity of the initial input state. So through a homodyne detection on the final output phase-shift coherent state, one can get the parity and realize the HP gate.

### IV. QUANTUM ENTANGLEMENT DISTRIBUTION

In this section, we will show thoroughly how to realize an  $n$ -qubit HP gate and use it for entanglement distribution among distant quantum nodes, including  $n$ -qubit GHZ state  $|GHZ_n\rangle$ , W state  $|W_n\rangle$ , Dicke state  $|D_{n,k}\rangle$ , and certain sums of Dicke states  $|G_{n,k}\rangle$ . The entangled states  $|D_{n,k}\rangle$  and  $|G_{n,k}\rangle$  have the following forms

$$\begin{aligned} |D_{n,k}\rangle &= \frac{1}{\sqrt{C_n^k}} \sum \tilde{P}_k \left( |0\rangle^{\otimes(n-k)} |1\rangle^{\otimes k} \right), \\ |G_{n,k}\rangle &= \begin{cases} (|D_{n,k}\rangle + \sigma_x^{\otimes n} |D_{n,k}\rangle) / \sqrt{2}, & n \neq 2k; \\ |D_{2k,k}\rangle, & n = 2k, \end{cases} \quad (9) \end{aligned}$$

where  $C_n^k = n!/[k!(n-k)!]$ , the sum in the Dicke state is over all  $C_n^k$  permutations (produced by the permutation operator  $\tilde{P}_k$ ) with  $k$  qubits in the state  $|1\rangle$ , and  $\sigma_x$  is the bit flip operation. Note that the W state  $|W_n\rangle$  is a special case of Dicke state  $|D_{n,k}\rangle$  with  $k = 1$ . In the subsequent text, we will firstly give some detailed examples for the distribution of all the above entanglement with the HP

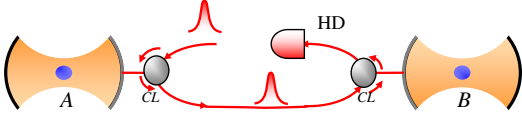


FIG. 3: (Color online) Setup for the two-qubit hybrid parity gate.  $CL$  is an optical circulator.

gate, and then make a generalization to get the  $n$ -qubit HP gate.

### A. Two-qubit case

As shown in Fig. 3, two distant single atoms  $A$  and  $B$  are trapped in two separated cavities. We assume the two single atoms are initially in the product state  $|\Psi_2\rangle_i = |+\rangle^{\otimes 2}$ . If the input optical pulse is prepared in a coherent state  $|\alpha\rangle$ , the initial state of the whole system can be written as  $|\Psi_2\rangle_i \otimes |\alpha\rangle$ . The input coherent optical pulse interacts sequentially with the two distant atoms confined in the respective cavities. It means that the coherent pulse undergoes two CPS gates as shown in Fig. 2. Then the final state of the system is

$$|\chi_2\rangle_s = \frac{1}{2} (|01\rangle_{AB} + |10\rangle_{AB}) \left| \alpha e^{i(\varphi_0 + \varphi_1)} \right\rangle + \frac{1}{2} (|00\rangle_{AB} \left| \alpha e^{2i\varphi_0} \right\rangle + |11\rangle_{AB} \left| \alpha e^{2i\varphi_1} \right\rangle). \quad (10)$$

In the case of low- $Q$  cavity ( $\kappa \gg \gamma$ ), we set the phase shift  $\varphi_0 = \pi/2$  and  $\varphi_1 = -\pi/2$  by adjusting  $\delta_1 = \delta_2 = \kappa/2$  and  $g = \kappa/\sqrt{2}$ . The state of the system in this case becomes

$$|\chi_2\rangle_s = \frac{1}{\sqrt{2}} (|\phi^+\rangle_{AB} |-\alpha\rangle + |\psi^+\rangle_{AB} |\alpha\rangle), \quad (11)$$

where  $|\phi^+\rangle_{AB} = (|00\rangle_{AB} + |11\rangle_{AB})/\sqrt{2}$  and  $|\psi^+\rangle_{AB} = (|01\rangle_{AB} + |10\rangle_{AB})/\sqrt{2}$  are the Bell states. One can get the parity of the initial state of the atoms through discriminating the two coherent states  $|\alpha\rangle$  and  $|-\alpha\rangle$ , and project the two distant atoms into a Bell state. Such discrimination can be achieved by a standard homodyne detection [35–37]. Here we choose a homodyne measurement on the position quadrature of the coherent state  $X = (a + a^\dagger)/\sqrt{2}$ . The wavefunction of coherent state in the position space is

$$\langle x | \alpha e^{i\theta} \rangle = (1/\pi)^{1/4} \exp[-(x - \sqrt{2} \cos \theta \alpha)^2/2 + i\zeta(x, \theta)], \quad (12)$$

$$\zeta(x, \theta) = [\alpha \sin \theta (x - 2\alpha \cos \theta)] \bmod 2\pi,$$

where  $\alpha$  is real,  $|x\rangle$  is an eigenstate of  $X$  with eigenvalue  $x$ . Then the Eq. (11) can be rewritten as

$$|\chi_2\rangle_s = \frac{1}{\sqrt{2}} (f(x, -\alpha) |\phi^+\rangle_{AB} + f(x, \alpha) |\psi^+\rangle_{AB}), \quad (13)$$

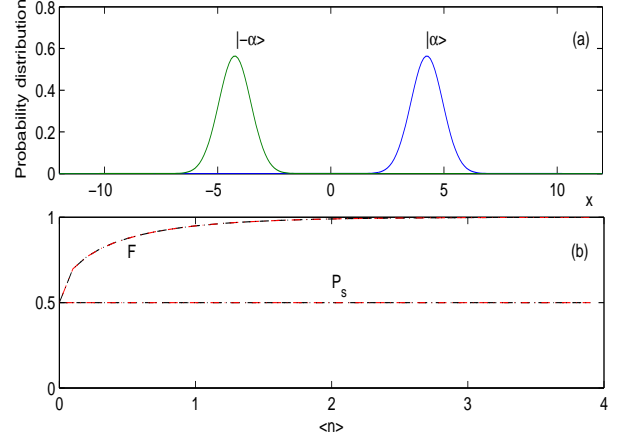


FIG. 4: (Color online) (a) The probability distribution for the final output phase-shift coherent states  $|\pm\alpha\rangle$ , with  $\alpha = 3$ . (b) shows the calculated success probability and fidelity of the final projected atomic entanglement  $|\psi^+\rangle_{AB}$  for the atomic spontaneous rates  $\gamma = 0$  (dashed curve),  $\gamma = 0.2\kappa$  (dash-dot curve) and  $\gamma = 0.5\kappa$  (dotted curve). Here we consider the channel transmission  $\eta^2 = 2/3$ .

where  $f(x, \pm\alpha) = (1/\pi)^{1/4} \exp[-(x \mp \sqrt{2}\alpha)^2/2]$  are two Gaussian curves corresponding to the coherent state  $|\pm\alpha\rangle$ . The midpoint of the two peaks of the curves is located at  $x_m = 0$  and the distance between the two peaks is  $x_d = 2\sqrt{2}\alpha$ . Upon the homodyne detection, we obtain the parity and the final projected atomic entanglement as the following

$$\begin{aligned} \mathbf{p} &= 1 \text{ and } |\Psi_2\rangle_f = |\psi^+\rangle_{AB} \text{ for } x \geq x_m; \\ \mathbf{p} &= 0 \text{ and } |\Psi_2\rangle_f = |\phi^+\rangle_{AB} \text{ for } x < x_m. \end{aligned} \quad (14)$$

As shown in Fig. 4(a), if the distance  $x_d$  is not too small, one can distinguish the two probability distributions with high fidelity by the homodyne detection. However, there are some photon losses in practice, which involve contributions from the channel attenuation, the nonideal cavity loss and atomic spontaneous emission. For simplicity, the channel attenuation is referred to as external loss, and the nonideal cavity loss and atomic spontaneous emission are referred to as internal loss. These photon losses will reduce the distinguishability in the homodyne detection. For long-distance entanglement distribution in our scheme, the external loss is the dominant photon loss and can be quantified with the parameter  $1 - \eta^2$ , where  $\eta^2$  is the efficient channel transmission. In the following discussion, we neglect the internal loss first but come back to it later using numerical simulation.

From the Eq. (14), the atoms will be projected into the Bell state  $|\psi^+\rangle_{AB}$  by the homodyne detection with the measure result  $x \geq x_m$ . After considering the channel

loss, the success probability of such an event is

$$P_s = \int_{x_m}^{+\infty} dx \operatorname{tr}_{\text{atom}}[\rho(x)]$$

$$= \frac{\operatorname{erfc}(\sqrt{2}\eta\alpha) + \operatorname{erfc}(-\sqrt{2}\eta\alpha)}{4}, \quad (15)$$

where  $\rho(x)$  is the density matrix of final state of the system,  $\operatorname{erfc}$  is the complementary error function. However, as shown in Fig. 4(a), the probability distribution with respect to the coherent state  $|\alpha\rangle$  also contributes to the measure result  $x \geq x_m$ , and it would have an influence on the fidelity of the projected Bell state  $|\psi^+\rangle_{AB}$ . Taking into account this imperfection, the average fidelity is calculated as [14]

$$F = \frac{1}{P_s} \int_{x_m}^{+\infty} dx_{AB} \langle \psi^+ | \rho(x) | \psi^+ \rangle_{AB}$$

$$= \frac{\operatorname{erfc}(-\sqrt{2}\eta\alpha)}{\operatorname{erfc}(\sqrt{2}\eta\alpha) + \operatorname{erfc}(-\sqrt{2}\eta\alpha)}. \quad (16)$$

With the channel transmission parameter  $\eta^2 = 2/3$ , the success probability and fidelity of the final projective state  $|\psi^+\rangle_{AB}$  are shown as a function of the mean photon number of the input coherent optical pulse in Fig. 4(b). In the situation of channel loss, the final phase-shift coherent state becomes  $|\pm\eta\alpha\rangle$  and their probabilities distribution are still symmetrical around the midpoint  $x_m = 0$ , hence the probabilities for the above two measurement results are the same and equal to  $1/2$ , which coincides with the numerical result in Fig. 4(b). The Fig. 4(b) also shows that the fidelity increases with the mean photon number of the input coherent state. Even in the presence of channel loss, one can get an ideal fidelity of the projective entanglement by increasing  $\alpha$ . For the initial input coherent optical pulse with  $\langle n \rangle = 3$ , a unit fidelity could be achieved as shown in Fig. 4(b). Note that the two probability distribution curves in Fig. 4(a) are highly symmetrical, so the success probability and fidelity of the distributed entanglement  $|\phi^+\rangle_{AB}$  is the same as  $|\psi^+\rangle_{AB}$ . Furthermore, we reconsider the atomic spontaneous  $\gamma$  in Eq. (2) and analyze numerically its influence on the fidelity and success probability of the projected entanglement. The performance of the parity gate is calculated with respect to  $\gamma = 0.2\kappa$  and  $0.5\kappa$ . The numerical result shown in Figure. 4(b) demonstrates that the influence of the atomic spontaneous emission on our scheme is very small, and the two-qubit parity gate is still with high fidelity and high success probability. For the nonideal cavity loss, it could be included through a modified atomic spontaneous emission rate [22].

### B. Three-qubit case

For the three-qubit case, we will build a three-qubit HP gate and exploit it for distributing various quantum entanglement, including the GHZ state, W state and Dicke

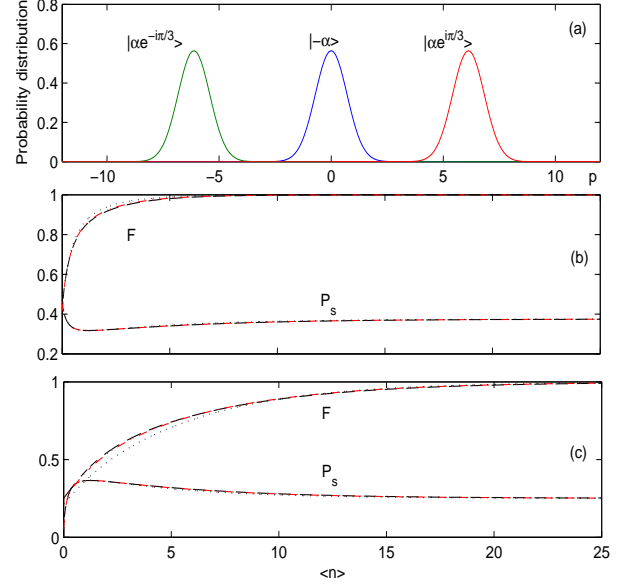


FIG. 5: (Color online) (a) The probability distribution for the final output phase-shift coherent states  $|\alpha\rangle$  and  $|\alpha e^{\pm i\pi/3}\rangle$ , with  $\alpha = 5$ . (b) and (c) show the calculated success probability and fidelity of the final projected atomic entanglement  $|W_3\rangle$  (or  $D_{3,2}$ ) and  $|GHZ_3\rangle$  for the atomic spontaneous rates  $\gamma = 0$  (dashed curve),  $\gamma = 0.2\kappa$  (dash-dot curve) and  $\gamma = 0.5\kappa$  (dotted curve), with the channel transmission  $\eta^2 = 2/3$ .

state. Like the configuration in Fig. 3, we assume three distant atoms confined in three separated low- $Q$  cavities, and the atoms are initially prepared in the product state  $|\Psi_3\rangle_i = |+\rangle^{\otimes 3}$ . An input coherent optical pulse experiences a CPS gate with each atom-cavity system as illustrated in Fig. 2. We adjust  $\delta_1 = \delta_2 = \sqrt{3}\kappa/2$  and  $g^2 = 3\kappa^2/2$ , and make the phase shift  $\varphi_0 = \pi/3$  and  $\varphi_1 = -\pi/3$  in the CPS gate, then the final state of the system can be written as

$$|\chi_3\rangle_s = \frac{1}{2} |GHZ_3\rangle |\alpha\rangle + \frac{\sqrt{6}}{4} |W_3\rangle |\alpha e^{i\pi/3}\rangle$$

$$+ \frac{\sqrt{6}}{4} |D_{3,2}\rangle |\alpha e^{-i\pi/3}\rangle. \quad (17)$$

In order to completely distinguish the above output phase-shift coherent states, we adopt the homodyne detection on the momentum quadrature of the coherent state  $P = (a - a^\dagger)/\sqrt{2}i$ . Using the wavefunction of the coherent state in the momentum space

$$\langle p | \alpha e^{i\theta} \rangle = (1/\pi)^{1/4} \exp[-(p - \sqrt{2} \sin \theta \alpha)^2 / 2 + i\zeta(p, \theta)],$$

$$\zeta(p, \theta) = \left[ -2\alpha \cos \theta (\sqrt{2}p - \alpha \sin \theta) \right] \bmod 2\pi, \quad (18)$$

where  $\alpha$  is real,  $|p\rangle$  is an eigenstate of  $P$  with eigenvalue  $p$ , the final state of the system can be rewritten as

$$\begin{aligned}
|\chi_3\rangle_s &= \frac{1}{2}f(p, 0)e^{i\zeta(p, \pi)}|GHZ_3\rangle \\
&+ \frac{\sqrt{6}}{4}f\left(p, \sqrt{3}\alpha/2\right)e^{i\zeta(p, \pi/3)}|W_3\rangle \\
&+ \frac{\sqrt{6}}{4}f\left(p, -\sqrt{3}\alpha/2\right)e^{i\zeta(p, -\pi/3)}|D_{3,2}\rangle, \quad (19)
\end{aligned}$$

where  $f(p, \beta) = (1/\pi)^{1/4} \exp[-(p - \sqrt{2}\beta)^2/2]$ ,  $\beta = 0, \pm\sqrt{3}\alpha/2$ . In Fig. 5(a), we have plotted the probability distribution for the output phase-shift coherent state  $|\alpha e^{i\theta}\rangle$ ,  $\theta = \pi, \pm\pi/3$ . The midpoints between the peaks of the probability distribution for  $|\alpha e^{\pm i\pi/3}\rangle$  and for  $|\alpha e^{i\pi}\rangle$  are located at  $p_{m\pm} = \pm\sqrt{6}\alpha/4$ . After the homodyne detection, the parity and final projected atomic entanglement are

$$\begin{aligned}
\mathbf{p} &= 1 \text{ and } |\Psi_3\rangle_f = |W_3\rangle \text{ for } p > p_{m+}; \\
\mathbf{p} &= 0 \text{ and } |\Psi_3\rangle_f = |GHZ_3\rangle \text{ for } p_{m-} \leq p \leq p_{m+}; \\
\mathbf{p} &= 2 \text{ and } |\Psi_3\rangle_f = |D_{3,2}\rangle \text{ for } p < p_{m-}. \quad (20)
\end{aligned}$$

As the two-qubit case, we also consider the influence of the channel loss and calculate the success probability and fidelity. The result is shown in Fig. 5(b) and (c). When the amplitude of the input coherent state  $\alpha = 5$ , as one would expect from the Eq. (19), the success probability for the final projected entanglement  $|W_3\rangle$  or  $|D_{3,2}\rangle$  is  $P_s = 3/8$ , for  $|GHZ_3\rangle$  is  $P_s = 1/4$ , and all the fidelities can approach unit. The figure 5(b) and (c) also show that the entanglement distribution can still be achieved with high fidelity and high success probability even in the presence of the atomic spontaneous emission.

### C. Distribution of sums of Dicke state

The sum of Dicke states  $|G_{n,k}\rangle$  has been recently introduced in [20] for quantum secret sharing. The most important step for this purpose is the distribution of quantum entanglement among distant parties. For a particular case, the distribution of  $|G_{3,1}\rangle$  is shown in the next. Instead of  $P$ , the homodyne measurement on the position quadrature  $X$  of the final output coherent state in Eq. (17) is applied. After such measurement, the state of the system becomes

$$|\chi_3\rangle_s = \frac{1}{2} \left( f(x, -\alpha)|GHZ_3\rangle + \sqrt{3}f(x, \alpha/2)|G'_{3,1}\rangle \right), \quad (21)$$

where  $f(x, \beta) = (1/\pi)^{1/4} \exp[-(x - \sqrt{2}\beta)^2/2]$ ,  $\beta = -\alpha, \alpha/2$ ,  $|G'_{3,1}\rangle = [e^{i\zeta(x, \pi/3)}|D_{3,1}\rangle + e^{-i\zeta(x, \pi/3)}|D_{3,2}\rangle]/\sqrt{2}$ . We have plotted the probability distribution for the output phase-shift coherent states in Fig. 6(a). The probability

distribution for the output coherent states  $|\alpha e^{\pm i\pi/3}\rangle$  in the position space are the same, so one cannot determine which Dicke entanglement is projected. This yields the sum of Dicke states  $|G'_{3,1}\rangle$ , which can be transformed into the standard form  $|G_{3,1}\rangle$  as shown in Eq. (9) through local unitary operations. The midpoint between the peaks of the probability distribution for  $|\alpha e^{\pm i\pi/3}\rangle$  and  $|\alpha e^{i\pi}\rangle$  is located at  $x_m = -\sqrt{2}\alpha/4$ . Thus the projected atomic entangled states are

$$\begin{aligned}
|\Psi_3\rangle_f &= |G'_{3,1}\rangle \text{ for } x \geq x_m; \\
|\Psi_3\rangle_f &= |GHZ_3\rangle \text{ for } x < x_m. \quad (22)
\end{aligned}$$

The success probability and fidelity for the two projected entanglement are plotted in Fig. 6(b) and (c). It is found that, only using an initial input coherent state with  $\langle n \rangle = 5$ , the success probability and fidelity for the final projected sum of Dicke state or GHZ state could be the ideal case as predicted in Eq. (21), i.e.  $P_s(|G'_{3,1}\rangle) = 3/4$ ,  $P_s(GHZ_3) = 1/4$ , and  $F(GHZ_3) = F(|G'_{3,1}\rangle) = 1$ . The numerical results in Fig. 6(b) and (c) also indicate that the atomic spontaneous emission has no significant effect on the performance of the parity gate and one can complete entanglement distribution with high fidelity and high success probability.

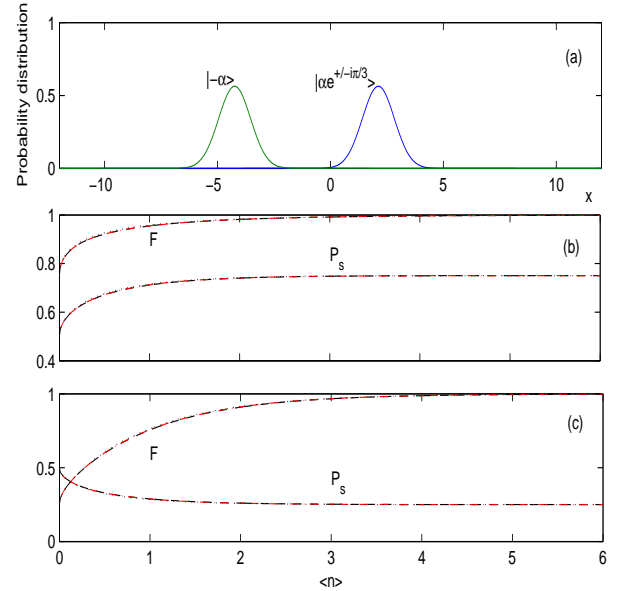


FIG. 6: (Color online) (a) The probability distribution for the final output phase-shift coherent states  $|\alpha\rangle$  and  $|\alpha e^{\pm i\pi/3}\rangle$ , with  $\alpha = 3$ . (b) and (c) show the calculated success probability and fidelity of the final projected atomic entanglement  $|G'_{3,1}\rangle$  and  $|GHZ_3\rangle$  for the atomic spontaneous rates  $\gamma = 0$  (dashed curve),  $\gamma = 0.2\kappa$  (dash-dot curve) and  $\gamma = 0.5\kappa$  (dotted curve), with the channel transmission  $\eta^2 = 2/3$ .

### D. $n$ -qubit generalization

According to the above detailed examples, we make a brief generalization to construct the  $n$ -qubit HP gate and show its use for entanglement distribution. Firstly, we assume  $n$  single atoms trapped in separated cavities are initially prepared in the state  $|+\rangle^{\otimes n}$ . An input coherent optical pulse, which is initiated in the coherent state  $|\alpha\rangle$ , interacts with each atom by a CPS gate. In the CPS gate, we set the phase shift  $\varphi_0 = \pi/n$  and  $\varphi_1 = -\pi/n$  by adjusting the parameters of the cavity-atom system. The final state of the system can be written as

$$|\chi_n\rangle_s = \frac{1}{\sqrt{2^n}} \left( \sqrt{2} |GHZ_n\rangle |-\alpha\rangle + \sum_{k=1}^{n-1} \sqrt{C_n^k} |D_{n,k}\rangle \left| \alpha e^{i(1-2k/n)\pi} \right\rangle \right). \quad (23)$$

Now if we perform the homodyne detection on the momentum quadrature  $P$  of the final output phase-shift coherent state, the  $n$  atoms would be projected into a GHZ state  $|GHZ_n\rangle$  ( $\mathbf{p}=0$ ) or Dicke state  $|D_{n,k}\rangle$  ( $\mathbf{p}=k$ ). Note that for  $n = 2k$ , one needs an additional HP gate with homodyne detection on the position quadrature  $X$  to distinguish the symmetric Dicke state  $|D_{2k,k}\rangle$  and the GHZ state  $|GHZ_{2k}\rangle$ . Besides, if we initially perform a homodyne detection on the position quadrature  $X$  of the output phase-shift coherent state in Eq. (23), the  $n$  atoms would be projected into a GHZ state  $|GHZ_n\rangle$  or certain sums of Dicke states  $|G_{n,k}\rangle$  which could be used for quantum secret sharing [20]. Because  $|W_n\rangle = |D_{n,1}\rangle = \sigma_x^{\otimes n} |D_{n,n-1}\rangle$ , the success probability for preparing W state in our scheme is  $P_s = n/2^{n-1}$ , which keeps an exponential gain over the scheme in [38].

As we know, the GHZ state and Dicke state (including the W state) are not equivalent under stochastic local operations and classical communication (SLOCC) [39]. This classification is particularly relevant for evaluating the use of states for multiparty quantum communication since states of the same SLOCC class can be used for the same applications. Several of two inequivalent entangled states above have been experimentally observed, like the GHZ state  $|GHZ_6\rangle$  [40] and W state  $|W_8\rangle$  [41] in ion trap system, and the Dicke state  $|D_{4,2}\rangle$  [42],  $|D_{6,3}\rangle$  [43] in linear-optical system. However, all these experiments are tailored to a particular entanglement, and can not provide a choice between different SLOCC inequivalent entanglement. In contrast, our scheme here gives a flexible physical way for preparing SLOCC inequivalent entanglement, which has also been presented recently in linear-optical system [44].

### V. DISCUSSION AND CONCLUSION

Before ending the paper, we give a brief discussion on the requirement of atom-cavity system in the two-

and three-qubit parity gate. First, in either case, the detuning of the input coherent optical pulse with respect to the atomic resonance and the cavity mode  $\delta_1$  and  $\delta_2$  are required to be the same. This could be satisfied by employing a resonant interaction between the atom and the cavity mode with  $\omega_c = \omega_0$ . Then one can change the frequency of the input coherent light  $\omega_p$  to achieve the desired detuning. Meanwhile, the atom-cavity coupling strength should be a required rate. For a Fabry-Perot cavity, the actual atom-cavity coupling strength depends on the atomic position through  $g(\mathbf{r}) = g_0 \cos(k_c z) \exp[-r_\perp^2/w_c^2]$ , where  $g_0$  is the peak coupling rate,  $r_\perp$  is the radial distance of the atoms with respect to the cavity axis,  $w_c$  and  $k_c$  are the width and the wave vector of the Gaussian cavity mode. Recent experiments have demonstrated the ability to manipulate the position of a single atom [45, 46] or a BEC [47] relative to the cavity mode using an atomic conveyor. With this experimental technology, the atom-cavity coupling strength can be tuned to control the reflectivity of the input coherent optical pulse. Note that such experiment has been performed recently using a quantum dot confined in a photonic crystal cavity [48]. Moreover, the similar controlled phase shifts up to  $\pi/4$  have also been observed in the same system [49]. So our scheme fits the current experimental technologies very well and could be feasible for large-scale quantum computation and quantum communication in the future.

In conclusion, with single atoms trapped in separated low- $Q$  cavities working in the intermediate coupling region as quantum nodes and a coherent optical pulse as quantum channel, we have proposed a scheme for atomic entanglement distribution over different nodes using a HP gate. In our scheme, through an input coherent optical pulse reflecting from a quantum node, a CPS gate between the atom and the coherent pulse is generated. With the CPS gate and homodyne detection, we have shown how to construct an  $n$ -qubit HP gate, and found that the HP gate is very flexible for preparing and distributing various interesting entanglement among different nodes, like GHZ state  $|GHZ_n\rangle$ , W state  $|W_n\rangle$ , Dicke state  $|D_{n,k}\rangle$  and certain sums of Dicke states  $|G_{n,k}\rangle$ . Our scheme is within the present-day experiment technology as it does not need strong coupling cavity and single-photon source. Even in the presence of channel loss and atomic spontaneous emission, the scheme can work with high success probability and high fidelity. In addition, the HP gate here has also an inherent distribution feature, it may function as a basic building block for a distributed QIP network.

### VI. ACKNOWLEDGMENT

This work is supported by the National Natural Science Foundation of China under Grant No. 60978009, the National Basic Research Program of China ("973" Program) (2007CB925204 and 2009CB929604), and NUS

- 
- [1] H.J. Kimble, *Nature (London)* **453**, 1023 (2008).
- [2] A.K. Ekert, *Phys. Rev. Lett.* **67**, 661 (1991).
- [3] H.J. Briegel, W. Dür, J.I. Cirac, and P. Zoller, *Phys. Rev. Lett.* **81**, 5932 (1998).
- [4] R. Cleve, D. Gottesman, and H.-K. Lo, *Phys. Rev. Lett.* **83**, 648 (1999).
- [5] J.I. Cirac, P. Zoller, H.J. Kimble, H. Mabuchi, *Phys. Rev. Lett.* **78**, 3221 (1997).
- [6] V. Giovannetti, S. Lloyd, L. Maccone, *Science* **306**, 1330 (2004).
- [7] D. Illuminati, *Nature Phys.* **2**, 803 (2006).
- [8] S. Bose, P.L. Knight, M.B. Plenio, and V. Vedral, *Phys. Rev. Lett.* **83**, 5158 (1999).
- [9] X.-L. Feng, Z.-M. Zhang, X.-D. Li, S.-Q. Gong, and Z.-Z. Xu, *Phys. Rev. Lett.* **90**, 217902 (2003); L.-M Duan and H.J. Kimble, *Phys. Rev. Lett.* **90**, 253601 (2003); D.E. Browne, M.B. Plenio, and S.F. Huelga, *Phys. Rev. Lett.* **91**, 067901 (2003).
- [10] C. Simon, and W.T.M. Irvine, *Phys. Rev. Lett.* **91**, 110405 (2003).
- [11] L.-M. Duan, M. D. Lukin, J. I. Cirac, and P. Zoller, *Nature (London)* **414**, 413 (2001).
- [12] L. Childress, J.M. Taylor, A.S. Sørensen, and M.D. Lukin, *Phys. Rev. Lett.* **96**, 070504 (2006).
- [13] E.S. Polzik, J. Carri, and H.J. Kimble, *Phys. Rev. Lett.* **68**, 3020 (1992).
- [14] P. van Loock, T.D. Ladd, K. Sanaka, F. Yamaguchi, K. Nemoto, W.J. Munro, and Y. Yamamoto, *Phys. Rev. Lett.* **96**, 240501 (2006).
- [15] T.D. Ladd, P. van Loock, K. Nemoto, W.J. Munro, and Y. Yamamoto, *New J. Phys.* **8**, 184 (2006).
- [16] C.H. Bennett and S.J. Wiesner, *Phys. Rev. Lett.* **69**, 2881 (1992).
- [17] N. Gisin, G. Ribordy, W. Tittel, and H. Zbinden, *Rev. Mod. Phys.* **74**, 145 (2002).
- [18] C.H. Bennett, G. Brassard, C. Crépeau, R. Jozsa, A. Peres, and W.K. Wootters, *Phys. Rev. Lett.* **70**, 1895 (1993).
- [19] M. Muraio, D. Jonathan, M.B. Plenio, and V. Vedral, *Phys. Rev. A* **59**, 156 (1999).
- [20] A. Sen(De), U. Sen, and M. Żukowski, *Phys. Rev. A* **68**, 032309 (2003).
- [21] S.S. Ivanov, P.A. Ivanov, I.E. Linington, and N.V. Vitanov, *Phys. Rev. A* **81**, 042328 (2010).
- [22] L.-M. Duan and H.J. Kimble, *Phys. Rev. Lett.* **92**, 127902 (2004).
- [23] J. Cho and H.W. Lee, *Phys. Rev. Lett.* **95**, 160501 (2005).
- [24] P. Xue and Y.-F. Xiao, *Phys. Rev. Lett.* **97**, 140501 (2006).
- [25] F. Mei, M. Feng, Y.-F. Yu, and Z.-M. Zhang, *Phys. Rev. A* **80**, 042319 (2009).
- [26] J.-H An, M. Feng, and C. H. Oh, *Phys. Rev. A* **79**, 032303 (2009).
- [27] Q. Chen and M. Feng, *Phys. Rev. A* **79**, 064304 (2009).
- [28] F. Mei *et al.*, *Europhys. Lett.* **91**, 10001 (2010).
- [29] T.B. Pittman, B.C. Jacobs, and J.D. Franson, *Phys. Rev. A* **64**, 062311 (2001).
- [30] C.W.J. Beenakker *et al.*, *Phys. Rev. Lett.* **93**, 020501 (2004).
- [31] A. Kolli *et al.*, *Phys. Rev. Lett.* **97**, 250504 (2006); B. Trauzettel *et al.*, *Phys. Rev. B* **73**, 235331 (2006); K. Lalumière *et al.*, *Phys. Rev. A* **81**, 040301(R) (2010).
- [32] R. Ionicioiu, *Phys. Rev. A* **75**, 032339 (2007).
- [33] Simon J. Devitt *et al.*, *Phys. Rev. A* **76**, 052312 (2007).
- [34] Radu Ionicioiu, A.E. Popescu, W.J. Munro, and T.P. Spiller, *Phys. Rev. A* **78**, 052326 (2008).
- [35] B. Yurke and D. Stoler, *Phys. Rev. Lett.* **57**, 13 (1986).
- [36] K. Nemoto and W. J. Munro, *Phys. Rev. Lett.* **93**, 250502 (2004).
- [37] S.G.R. Louis, K. Nemoto, W.J. Munro, and T.P. Spiller, *New J. Phys.* **9**, 193 (2007).
- [38] T. Tashima *et al.*, *Phys. Rev. A* **77**, 030302(R) (2008).
- [39] F. Verstraete *et al.*, *Phys. Rev. A* **65**, 052112 (2002); A. Sen(De) *et al.*, *ibid.* **68**, 062306 (2003).
- [40] D. Leibfried *et al.*, *Nature (London)* **438**, 639 (2005).
- [41] H. Häffner *et al.*, *Nature (London)* **438**, 643 (2005).
- [42] N. Kiesel *et al.*, *Phys. Rev. Lett.* **98**, 063604 (2007).
- [43] R. Prevedel *et al.*, *Phys. Rev. Lett.* **103**, 020503 (2009); W. Wieczorek *et al.*, *ibid.* **103**, 020504 (2009).
- [44] W. Wieczorek, N. Kiesel, C. Schmid, and H. Weinfurter, *Phys. Rev. A* **79**, 022311 (2009).
- [45] K.M. Fortier *et al.*, *Phys. Rev. Lett.* **98**, 233601 (2007).
- [46] S. Nußmann *et al.*, *Phys. Rev. Lett.* **95**, 173602 (2005).
- [47] Y. Colombe *et al.*, *Nature (London)* **450**, 268 (2007).
- [48] D. Englund *et al.*, *Nature (London)* **450**, 857 (2007).
- [49] I. Fushman *et al.*, *Science* **320**, 769 (2008).